Journal of Materials Chemistry A

Simultaneous removal of C2H2 and C2H6 for C2H4 purification by robust MOFs featuring high density of heteroatoms

Journal:	*Journal of Materials Chemistry A*
Manuscript ID	TA-ART-03-2023-001598.R2
Article Type:	Paper
Date Submitted by the Author:	26-Aug-2023
Complete List of Authors:	Xian, Shikai; Shenzhen Polytechnic Peng, Junjie; South China University of Technology Pandey, Haardik; Wake Forest University, Physics Graham, Wells; Wake Forest University Yu, Liang ; South China University of Technology, School of Chemistry and Chemical Engineering Wang, Hao; Shenzhen Polytechnic, Hoffmann Institute of Advanced Materials Tan, Kui; University of Texas at Dallas, Department of Materials Science and Engineering Thonhauser, Timo; Wake Forest University, Department of Physics Li, Jing; Rutgers The State University of New Jersey, Chemistry and Chemical Biology

Simultaneous removal of C_2H_2 and C_2H_6 for C_2H_4 purification by robust MOFs featuring high density of heteroatoms

Shikai Xian,[a,b] Junjie Peng,[c] Haardik Pandey,[d] Wells Graham, [d] Liang Yu,[c] Hao Wang,[a] Kui Tan,[e] Timo Thonhauser,[d] Jing Li[b,a,*]

a. Hoffmann Institute of Advanced Materials, Shenzhen Polytechnic, 7098 Liuxian Boulevard., Shenzhen, Guangdong 518055, China
b. Department of Chemistry and Chemical Biology, Rutgers University, 123 Bevier Road, Piscataway, New Jersey 08854, USA
c. School of Environmental and Chemical Engineering, Foshan University, 18 Jiangwan 1st Road, Chancheng, Foshan 528000, China
d. Department of Physics and Center for Functional Materials, Wake Forest University, 1834 Wake Forest Road, Winston-Salem, North Carolina 27109, USA
e. Department of Chemistry, University of North Texas, Denton, Texas 76201, USA

Abstract:

Simultaneous removal of C_2H_6 and C_2H_2 from C_2H_4 streams is of great importance in petrochemical industry but remains a challenging task. To address this challenge, we have selected three isoreticular MOFs with high stability, low cost, as well as desirable scale-up ability, namely, MOF-303, MIL-160, and CAU-23 and assessed their potential in simultaneous removal of acetylene and ethane for ethylene purification. Each MOF exhibits desirable C_2H_2 and C_2H_6 uptake capacity (> 5.5 mmol/g and > 4 mmol/g, respectively), as well as good C_2H_2/C_2H_4 selectivity (> 2) and C_2H_6/C_2H_4 selectivity (> 1.5). Notably, the MOF-303 takes up 4.96 mmol/g of C_2H_6 at 298 K and 1 bar, the highest value among the three MOFs, with a C_2H_6/C_2H_4 selectivity in the range of 1.55~2.47. MIL-160 possesses a very high C_2H_2 uptake (9.1 mmol/g) and C_2H_2/C_2H_4 selectivity, 10.6, (1:1, v/v) at 298 K, much higher than all other MOFs tested to date for simultaneous removal of C_2H_6 and C_2H_2 from C_2H_4. The results from breakthrough experiments confirm that all three MOFs demonstrate excellent performance for C_2H_4 purification in ternary mixture of $C_2H_6/C_2H_4/C_2H_2$ (1:1:1, v/v/v). For MOF-303, MIL-

160, and CAU-23, polymer-grade C_2H_4 up to 0.164, 0.21, and 0.181mmol/g can be obtained from the equimolar ternary mixture in a single separation step from breakthrough experiment. Additionally, DFT calculations have been performed to further investigate the mechanism of the adsorption/separation for C_2H_6, C_2H_4, and C_2H_2.

Key Words: MOF-303; MIL-160; CAU-23; ethane-selective adsorbent; C_2H_2/C_2H_4/C_2H_6 separation; C_2H_4 purification; simultaneous removal of C_2H_2 and C_2H_6

1. Introduction

Ethylene (C_2H_4), one of the most important hydrocarbons used as feedstock to produce polyethylene, is generally produced from hydrocracking of fossil fuels[1, 2]. During this process, two inevitable impurities, ethane (C_2H_6) and acetylene (C_2H_2), must be removed due to their harmful effect on the subsequent polyethylene production. C_2H_2 is poisonous to the catalyst of C_2H_4 polymerization, which dramatically reduces the quality of the resulting polyethylene[3]. On the other hand, the presence of even small amount of C_2H_6 could lead to longer reaction times and marked decrease in the efficiency of polyethylene production[4]. It is thus of great importance and necessity to remove C_2H_6 and C_2H_2 from C_2H_4 streams in order to produce high quality polyethylene. Partial hydrogenation and solvent extraction are the current commercial approaches for removal of C_2H_2, however, these approaches not only need noble metal catalyst and large amount of organic solvent, but also require further purification of the C_2H_4 product to reach polymer grade[5, 6]. For the removal of C_2H_6, current state-of-the-art strategies rely on cryogenic distillations that operate at high pressure and low temperature and suffer from high energy consumption and high installation costs of the separation unites[7, 8].

As an alternative approach to cryogenic distillation, adsorptive separation using porous materials to purify C_2H_4 has demonstrated its eco-friendly and energy-efficient advantages[9]. Among diverse classes of porous materials, metal–organic frameworks

(MOFs), constructed by metal clusters and organic linkers, are of particular interest owing to their advantageous features, such as extra-high surface area, structural tunability, linker tailorability, and controllable properties, etc[10]. Recent studies have shown that MOFs exhibit superior separation performance for C_2H_4/C_2H_6 mixtures compared to traditional adsorbents such as zeolites[11-14]. However, for the vast majority of reported MOFs, especially those with open metal site (OMS) or π-complexation component, C_2H_4 is always preferentially adsorbed rather than C_2H_6, leading to not only substantial difficulty to obtain high-purity C_2H_4 but also higher energy cost as the more frequent adsorption-desorption switching[4, 15-17]. Ideally, MOFs for C_2H_4/C_2H_6 separation should be based on an ethane selective mechanism because C_2H_6 is identified as the impurity with much lower quantities compared to C_2H_4. Thus, ethane-selective MOFs would achieve apparently reduced energy consumption along with greatly simplified separation operation and the device. Current strategies for the development of ethane-selective materials mostly rely on strengthening van der Waals (VDWs) interactions between the hydrogen atoms of ethane and the heteroatoms of the organic linkers[8, 18-22]. However, ethane-selective MOFs reported so far remain scarce, and their uptake capacity and selectivity are yet to be improved. Therefore, seeking for high-performance ethane-selective MOFs is an important task to be pursued. Similarly, removing C_2H_2 from C_2H_4 streams by using MOF adsorbents could become a promising alternative to current commercial approaches due to lower energy cost and eco-friendly process[23]. Considering that ethane-selective MOFs can efficiently purify C_2H_4 by removing C_2H_6, and if choosing an ethane-selective MOF that can also selectively adsorb C_2H_2 over C_2H_4, simultaneous removal of C_2H_6 and C_2H_2 could be realized. Until now, only a few studies related to this approach have been reported[4, 5, 23-25], and in all cases, while high purity C_2H_4 was produced in a single breakthrough experiment, there are some issues remaining to be resolved. For example, the working capacity of C_2H_6 and/or C_2H_2 is not high enough, leading to a low throughput efficiency of high-purity C_2H_4 with regards to time. On the other hand, several MOFs developed in these studies feature good C_2H_6/C_2H_4 selectivity but poor C_2H_2/C_2H_4 selectivity. For

instance, according to the C_2H_2 breakthrough curves for NPU-1[24], NPU-2[24], and UPC-613[25], the C_2H_2 breakthrough times are shorter than that of C_2H_6, namely, C_2H_2 would elute from the adsorbent bed before C_2H_6, resulting in low yield of high-purity C_2H_4 in the simultaneous separation processes. Therefore, for simultaneous removal of C_2H_2 and C_2H_6, high C_2H_2 uptake capacity and selectivity are as important as high C_2H_6 uptake capacity and selectivity, which should be taken into consideration when developing new MOFs for this application. Generally, introducing OMS is an efficient strategy to design new MOFs with high C_2H_2 uptake and selectivity. However, this kind of MOFs generally exhibit ethylene selective feature owing to stronger electrostatic interaction between OMS and C_2H_4 than between OMS and C_2H_6 (e.g., Co-MOF-74[26], Cu-BTC[26], FJU-8[27]), so simultaneous removal of C_2H_2 and C_2H_6 cannot be accomplished. Hence, it seems of great difficulty to achieve simultaneously high C_2H_6/C_2H_4 and C_2H_2/C_2H_4 selectivity as well as high C_2H_6 and C_2H_2 uptake. One possible solution is to include heteroatoms in the ligands. Several earlier reports have shown that these heteroatoms may serve as strong adsorption site for C_2H_2 as a result of strong Lewis acid-base interaction between the Lewis basic site (heteroatom), and the acidic hydrogen atoms (at both ends of C_2H_2 molecule)[27-30]. Taking this into account, it is possible to obtain an ethane-selective MOF with high C_2H_2 uptake and selectivity by fine tuning the type and the amounts of heteroatoms, along with the pore structure.

Apart from separation performance, there are some other prerequisites that determine the feasibility for industrial applications, such as material cost, water/moisture stability and scale-up capability[31]. Stability, particularly water/moisture stability, is of great importance because it always determines the long-term storage/application and operational cost. Unfortunately, some ethane-selective MOFs such as $Ni(bdc)(ted)_{0.5}$ and IRMOF-8 feature high ethane uptake capacity but suffer from structural decomposition in humid air[32], significantly lessening the feasibility of their application. On the other hand, while many other ethane-selective MOFs show sufficient water/moisture stability, such as PCN-250[20], SNNU-40[33], and CPM-733[34], their ligands are quite expensive, which would seriously hinder their industrial

application when considering the economic feasibility. In addition, some ethane-selective MOFs synthesized in relative harsh conditions involving high temperature and pressure, large amount of template reagents, or complex steps usually suffer fromlow scale-up ability because the total cost of instrument, chemicals, as well as energy would be extremely high for the scale up processes. Hence, in developing or selecting ethane-selective MOFs to be utilized in simultaneous removal of C_2H_2 and C_2H_6 for C_2H_4 purification, we must consider simultaneously all the factors and find an optimal balance between separation performance, stability, and cost.

In this work, we selected three highly stable Al-based MOFs, namely, MOF-303, MIL-160, and CAU-23, all of which feature similar 1D channel but different heteroatoms, as ethane-selective adsorbents to address the challenging task of simultaneously removal of C_2H_6 and C_2H_2 from C_2H_4 streams. All three Al-MOFs were synthesized following reported procedures with modifications[35]. Adsorption isotherms were measured by volumetric method and used to calculate the corresponding ideal adsorbed solution theory (IAST) selectivity as well as the isosteric heats of adsorption. Ternary fixed bed breakthrough experiments were carried out to further confirm the potential for real-world applications. Finally, molecular simulations were performed to elucidate the adsorption mechanisms of C_2H_6, C_2H_4, and C_2H_2.

2. Material and Method

2.1 Reagents and solvents

All reagents were purchased commercially and used as received. Aluminum chloride hexahydrate was purchased from Alfa Aesar; 3,5-pyrazoledicarboxylic acid monohydrate, 2,5-furandicarboxylic acid, and 2,5-thiophenedicarboxylic acid were all supplied by TCI America; Sodium hydroxide was purchased from Acros Organics; The high-purity gases used in adsorption experiments were obtained from Praxair Inc. (New Jersey)

2.2 Preparation of MOF-303, MIL-160, and CAU-23

MOF-303 was prepared by using the procedure reported by Yaghi et al.[35] 1.04 g Aluminum chloride hexahydrate ($AlCl_3 \cdot 6H_2O$, 4.308 mmol) and 0.75 g 3,5-pyrazoledicarboxylic acid monohydrate (H_3PDC, 4.308 mmol) were dissolved in 72 mL water in a 200 mL glass flask, 3 mL aqueous NaOH (0.26 g, 6.5 mmol) were added dropwise to the above mixture under stirring. The flask was then heated at 100 ºC with reflux for 12h. After cooling down to room temperature, the as-synthesized MOF-303 powder was obtained by filtration. To remove the remaining 3,5-pyrazoledicarboxylic acid, the powder was washed thoroughly with water, followed by heated under vacuum at 150 ºC for 12h. MIL-160 and CAU-23 were obtained through the same process as that of MOF-303 by replacing the ligand 3,5-pyrazoledicarboxylic acid monohydrate with 2,5-Furandicarboxylic acid and 2,5-thiophenedicarboxylic acid, respectively.

2.3 Characterization

Powder X-ray diffraction (PXRD) patterns were collected on a Ultima IV X-ray diffractometer between a scanning range of 3°-35° at 2.0 deg/min. Thermogravimetric analysis (TGA) was performed on a TA Q5000-IR analyzer, with temperature increased at a ramping rate of 10 K/min from ambient temperature to 973 K under a flowing nitrogen environment. Nitrogen adsorption isotherms were obtained at 77 K using a Micromeritics 3Flex analyzer. The BET model was chosen to evaluate the specific surface area, while the HK (Horvath-Kawazoe) method was applied to acquire the micropore size distribution.

2.4 Hydrocarbon adsorption experiments

C_2H_6, C_2H_4, and C_2H_2 sorption isotherms were performed on the 3Flex analyzer. Volumetric sorption data were measured at various temperatures and pressures up to 1 bar. The desired temperature was controlled by employing water bath (298 K-323 K) circulated by a precise temperature thermostat. Prior to data collection, 80–100 mg samples were degassed at 423 K for 12 h.

2.5 Breakthrough experiments

Breakthrough curves were obtained on a home-made experimental setup (Fig. S1) at 298 K. Under the control of a mass flow meter, the velocity was set to be 1 mL/min for the ternary mixture $C_2H_6/C_2H_4/C_2H_2$ (1:1:1, v/v). A small-scale adsorption column was made by packing about 0.2 g of an activated sample into a long stainless hollow cylinder. The real time concentration of the effluent component was probed by a gas chromatography (GC) spectrometer (Agilent, 7890A). Before the experiment, the packed column was heated at 423 K under 5 mL/min He flow for 1h. After the breakthrough experiment, the desorption curves were measured at 298 K or 323 K under 5 mL/min He flow.

2.6 Theoretical calculation method

All *ab initio* calculations were performed using density functional theory (DFT) in VASP (Vienna Ab Initio Simulation Package)[36, 37], with vdW-DF functional[38-41] to take into account important van der Waals interactions. All the MOF unit cells were optimized by carrying out spin-polarized calculations, with SCF convergence of 0.1 meV and the plane wave energy cut-off set at 600 eV. The unit cell parameters and atoms were allowed to move till the force acting between atoms reached below 5 meV/Å. Potential binding sites were studied by placing C_2H_2, C_2H_4, and C_2H_6 molecules in the MOF-303, MIL-160, and CAU-23 at various sites and all the atoms were allowed to relax in accordance with the convergence condition. Difference in the total energies of the MOF unit-cell and the guest molecules was used to calculate the corresponding binding energies. Induced charge densities were also calculated that maps the variation in charge density upon introduction of the guest molecules and help identifying the interactions happening at the binding sites.

3. Results and Discussion

3.1 Characterization

MOF-303, MIL-160, and CAU-23 are built from infinite $Al(OH)(-COO)_2$ secondary building units (SBUs) linked through 3,5-pyrazoledicarboxylate, 2,5-furandicarboxylate, and 2,5-thiophenedicarboxylate, respectively. All three Al-MOFs

feature 1D channels with small differences. As shown in Fig. 1(a), MOF-303 contains a straight channel because the SBUs are connected alternately by equal number of cis- and trans- corner-sharing AlO_6 octahedra. The channel in CAU-23 is corrugated due to a large percent of trans- and small percent of cis- corner-sharing AlO_6 octahedra which form corresponding straight and helical sections in the infinite chain. For MIL-160, on the other hand, the SBUs are built only by cis- corner-sharing AlO_6 octahedra, forming a straight channel with alternate narrow and wide sections.

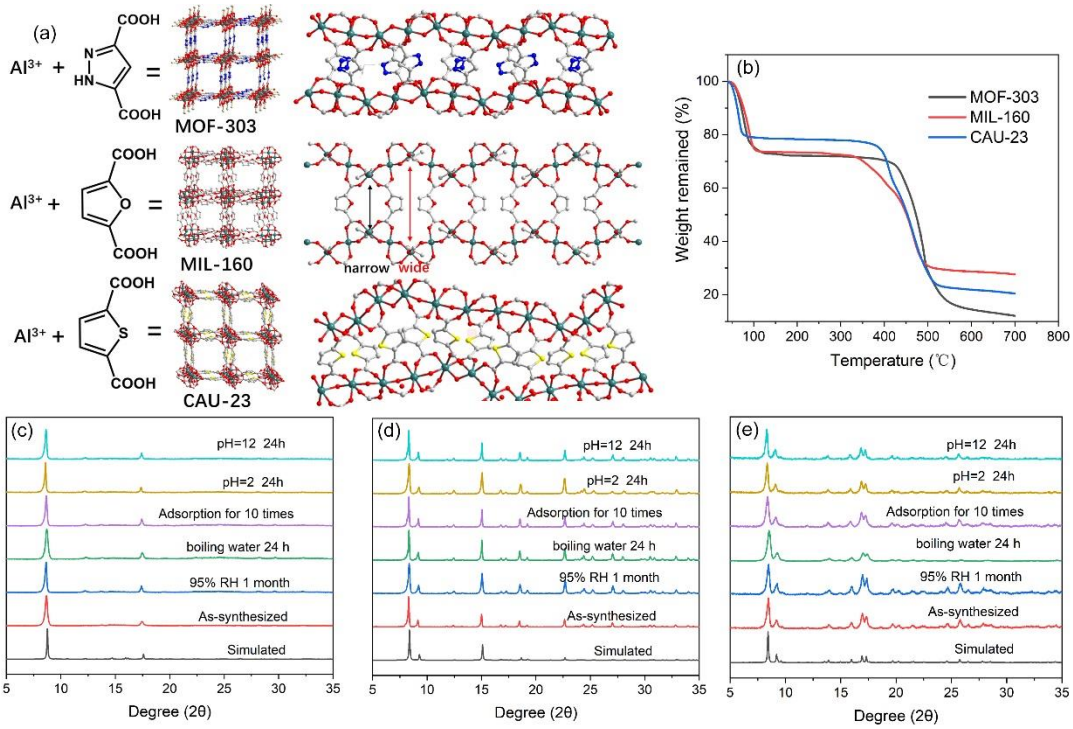

Fig. 1. (a) The composition and structure of MOF-303, MIL-160, and CAU-23 and the shape of pore windows and channels. (b) TG curves for MOF-303, MIL-160, and CAU-23. Simulated and experimental PXRD patterns of (c) MOF-303, (d) MIL-160, and (e) CAU-23 collected after being treated under different conditions.

The sample purity of all three Al-MOFs were confirmed by powder X-ray diffraction (PXRD) analysis, and as shown in Fig. 1(c)-1(e), the PXRD patterns of the as-synthesized MOFs match well with the corresponding simulated patterns. N_2 sorption experiments were conducted at 77 K to establish permanent microporosity of the MOFs. As expected, the three MOFs exhibit similar porosity due to their similar

pore structure, with the BET surface area of 1220 m^2/g, 1188 m^2/g, and 1242 m^2/g for MOF-303, MIL-160, and CAU-23, respectively (Figs. S2-S4), and pore size all in the range of 5~7.5 Å (Fig. S5). The high surface area and suitable pore size allow the channel to take up C_2H_6, C_2H_4, and C_2H_2 molecules with negligible diffusion hindrance. The thermal stability of the MOFs was evaluated by thermogravimetric (TG) analysis. As shown in Fig. 1(b), all three MOFs show two distinct weight loss steps: the first one before 125 ℃ corresponds to the weight loss of the solvent molecules, and the second one signifies the onset of framework decomposition beginning at 420 ℃, 350 ℃, and 380 ℃ for MOF-303, MIL-160, and CAU-23, respectively. Additionally, chemical stability was tested by comparing the PXRD patterns of samples before and after treated under different conditions, including in boiling water for 24 h and in aqueous solutions with pH = 2 and pH = 12 for 24 h (Fig. 1(c)-1(e)). The corresponding N_2 isotherms of the samples after being treated under different conditions were also measured at 77 K, and the results are plotted in Fig. S6. As evident from these figures, both the PXRD patterns as well as the N_2 isotherms show no apparent changes in all cases, revealing excellent structural stability of the three MOFs.

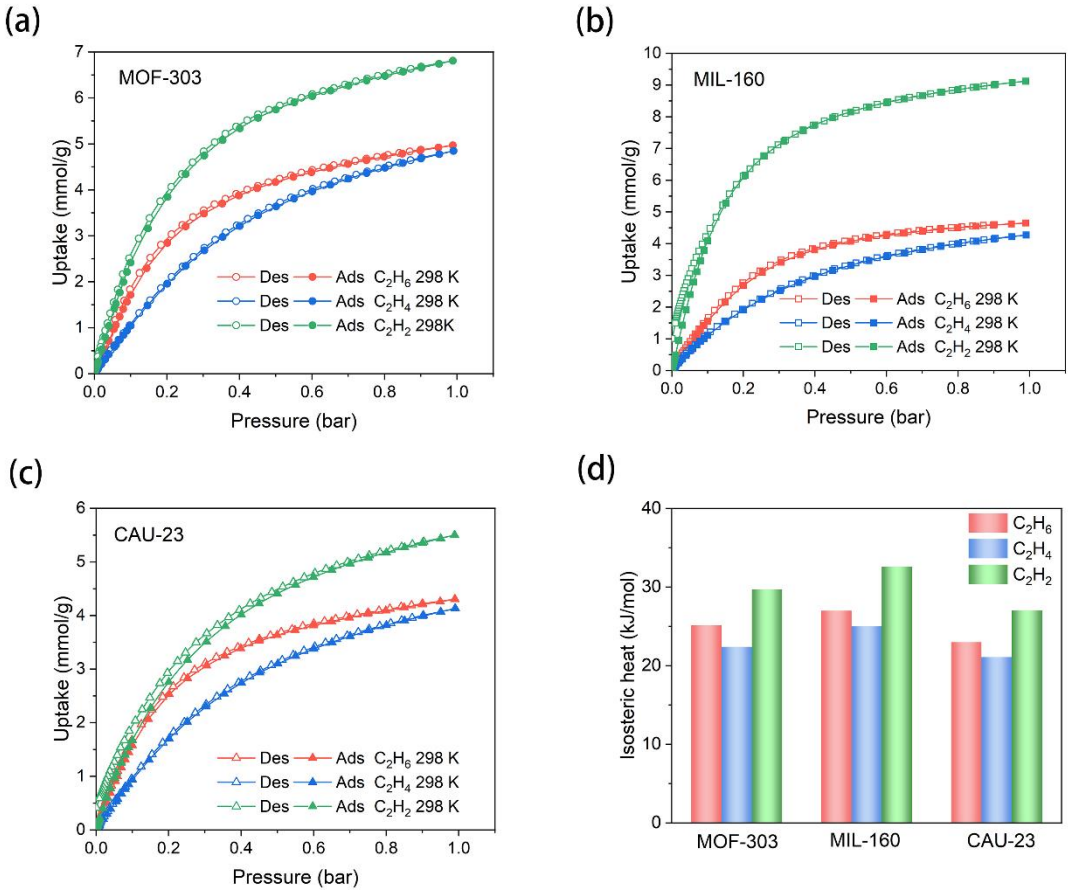

Fig. 2. C_2H_6, C_2H_4, and C_2H_2 adsorption-desorption isotherms of (a) MOF-303, (b) MIL-160, and (c) CAU-23 at 298 K. (d) Zero coverage isosteric heats for C_2H_6, C_2H_4, and C_2H_2 in MOF-303, MIL-160, and CAU-23.

3.2 Single-component adsorption isotherms of C_2H_2, C_2H_4, and C_2H_6 and selectivity

The flourishing cavity, suitable pore size, and highly stable structure of these MOFs encouraged us to further investigate their performance on $C_2H_2/C_2H_4/C_2H_6$ separation. First, static adsorption, regarded as the highly effective approach to evaluate adsorbent, was conducted upon MOF-303, MIL-160, and CAU-23. Adsorption isotherms of single component C_2H_6, C_2H_4, and C_2H_2 for the three MOFs were collected at 298 K, as presented in Fig. 2(a)-(c). In particular, all the C_2H_6 isotherms are type I with steep slopes, a typical feature of strong affinity towards adsorbates in microporous materials. The adsorbed amount of C_2H_6 is higher than that of C_2H_4 over the entire pressure range, indicating MOF-303, MIL-160, and CAU-23 are all ethane-selective. The C_2H_6 uptake

capacity is of great importance for ethane-selective MOF as it is closely related to production output of pure C_2H_4 per unit time[4]. At 298 K and 1 bar, MOF-303, MIL-160, and CAU-23 adsorb 4.96, 4.65, and 4.30 mmol/g of C_2H_6, respectively, which are higher than those of the majority of ethane-selective MOFs at the same conditions, such as $Fe_2(O_2)(dobdc)$[42], $Cu(Qc)_2$[43], and MAF-49[8], etc. The value 4.96 mmol/g for MOF-303 is lower than those of SNNU-40 (7.54 mmol/g)[33], CPM-733 (7.13 mmol/g)[34], and CPM-233 (7.45 mmol/g)[34] and slightly lower than those of $Ni(bdc)(ted)_{0.5}$ (5 mmol/g)[44] and PCN-250 (5.21mmol/g)[20]. We also obtained simulated adsorption isotherms of both C_2H_4 and C_2H_6 at 298 K for all three MOFs (MOF-303, MIL-160, CAU-23), which are generally consistent with the experimental data (Figs. S19-S21). Compared to the C_2H_6 and C_2H_4 isotherms, C_2H_2 isotherms of all the three MOFs exhibit the highest uptake in the tested pressure range, as shown in Fig. 2(a)-(c), indicating the strongest interaction between C_2H_2 molecule and the frameworks. The adsorbed amounts for MOF-303 and CAU-23 are as high as 6.81 and 5.50 mmol/g, respectively, exceeding many other ethane-selective MOFs. Particularly, the C_2H_2 uptake of MIL-160 reaches 9.12 mmol/g at 298 K, much higher than other ethane-selective MOFs and comparable with MOFs with highest acetylene uptakes, such as Co-MOF-74[27], FJI-H8[45], and ZJU-40a[28], which possess open metal sites. The isosteric heats of adsorption were calculated for the three gases over the entire coverage range (Fig. S32). For all three MOFs, the order $C_2H_2 > C_2H_6 > C_2H_4$, well with consistent with the isotherm data. Compared to MOF-303 and CAU-23, MIL-160 features the highest isosteric heats for all three gases, indicating the strongest interaction between the gas molecule and the framework, also in trend with the adsorption performance. The isosteric heats of C_2H_2 and C_2H_6 increase apparently with the coverage due to the strong H-bond between the C_2H_2 or C_2H_6 molecule. While for C_2H_4, the enhancement is not as obvious, which could be attributed to the weaker interaction between the C_2H_4 and the framework. The data at zero coverage are shown in Fig. 2(d), where for C_2H_2 the values are 32.6 kJ/mol (MIL-160) > 29.7 kJ/mol (MOF-303) > 27.0 kJ/mol (CAU-23). For C_2H_6, a similar order is observed: 25.1 kJ/mol (MIL-160) > 22.4 kJ/mol (MOF-303) > 21.1 kJ/mol (CAU-23). For C_2H_4,

as expected, the values are the lowest but also follow the same order: 28.32, 22.41, and 21.10 kJ/mol for MIL-160, MOF-303 and CAU-23, respectively. The order of isosteric heats may be ascribed to, at least partially, the different electronegativity of heteroatoms. For MIL-160, the O atom possesses the highest electronegativity leading to a strong C-H···O interaction, and the lower electronegativity of N and S gives rise to weaker interactions for MOF-303 and CAU-23.

It is noticed that although the ethane uptake amounts of PCN-250, CPM-733, CPM-233, and SNNU-40 are higher than those of MOF-303, MIL-160, and CAU-23 at 1 bar, the ligands of these MOFs are much more expensive than 3,5-pyrazoledicarboxylate, 2,5-furandicarboxylate, and 2,5-thiophenedicarboxylate in the title compounds, which would seriously hinder their industrial application when considering from economic feasibility. Additionally, it has been verified that these three Al-based MOFs are very easy to scale up in water at 373 K within 24 h[35]; however, for PCN-250, CPM-733, CPM-233, and SNNU-40, the complex synthesis steps, higher temperature, and non-aqueous solvent may lead to inevitable high cost in enlarging the production scale.

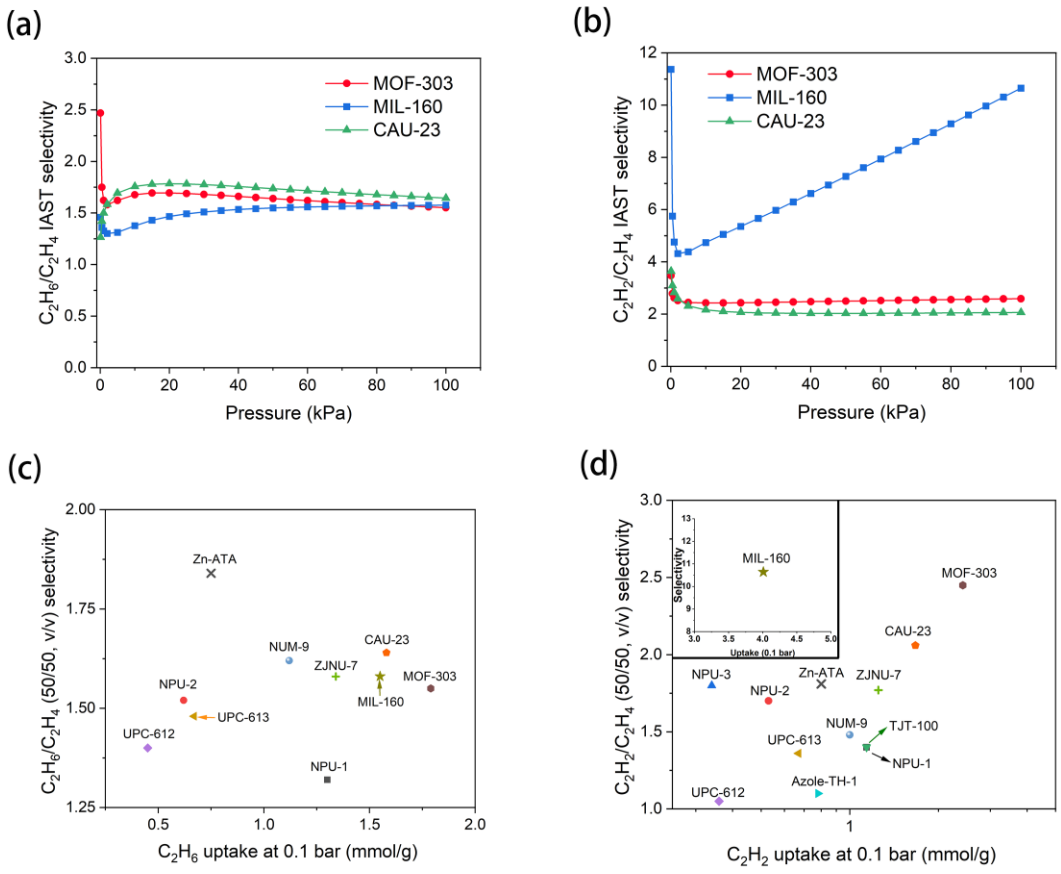

Fig. 3. IAST selectivity of (a) C_2H_6/C_2H_4 (1:1, v/v) and (b) C_2H_2/C_2H_4 (1:1, v/v) at 298K for MOF-303, MIL-160, and CAU-23. Comparison in (c) C_2H_6/C_2H_4 selectivity (50/50, v/v) and C_2H_6 uptake at 298 K and 0.1 bar and (d) C_2H_2/C_2H_4 selectivity (50/50, v/v) and C_2H_2 uptake at 298 K and 0.1 bar between these the three Al-MOFs and selected top-performing MOFs.

To further evaluate the separation property of the three MOFs for $C_2H_2/C_2H_6/C_2H_4$ mixture, IAST was employed to calculate the binary selectivities with the ratio of 1:1 (v/v, C_2H_6/C_2H_4 or C_2H_2/C_2H_4), and the results are shown in Fig. 3(a) and Fig. 3(b). The predicted selectivity of C_2H_6/C_2H_4 for MOF-303, MIL-160, and CAU-23 at 100 kPa are 1.55, 1.58, and 1.64, respectively, moderately high among the MOFs that have been tested for simultaneous removal of acetylene and ethane. For C_2H_2/C_2H_4, at 298 K and 100 kPa, while the values of MOF-303 and CAU-23 are already high, 2.59 and

2.06, respectively, the value for MIL-160 is 10.65, far surpassing MOF-303, CAU-23, and all the MOFs reported so far that have been evaluated for simultaneous removal of acetylene and ethane for ethylene purification. To intuitively assess the separation performance of MOF-303, MIL-160, and CAU-23, their uptake and selectivity values are compared with those of previously reported MOFs. Notably, the uptakes of C_2H_2 and C_2H_6 at 0.1 bar are chosen rather than that at 1 bar because the amounts of C_2H_2 and C_2H_6 in the gas mixtures after hydrocracking of fossil fuels are small, which is closer to reality. As shown in Fig. 3(c), the C_2H_6/C_2H_4 selectivity for MOF-303, MIL-160, and CAU-23 are lower than Zn-ATA, and comparable with NUM-9 and ZJNU-7 but higher than other MOFs. For C_2H_6 uptake at 298 K and 0.1 bar, MOF-303, CAU-23, and MIL-160 show distinct advantage as their C_2H_6 uptake capacity is higher than all other MOFs, as shown in Fig. 3(c). For C_2H_2/C_2H_4 selectivity and C_2H_2 uptake at 0.1 bar, MOF-303 and CAU-23 apparently outstrip all the other MOFs except MIL-160. The C_2H_2/C_2H_4 selectivity and C_2H_2 uptake at 0.1 bar are up to 10.64 and 4.01 mmol/g, respectively, as shown in Fig. 3(d). The appreciable C_2H_2 uptake, along with the high C_2H_2/C_2H_4 selectivity and C_2H_2 isosteric heat may be attributed to the specific basic-acid specific interaction between the two acidic hydrogen atoms at both ends of C_2H_2 and the high density of Lewis basic heteroatom sites fully exposed on the surface of the 1D channel, forming strong H-C≡C-H···M(heteroatom in the ligands) hydrogen bonding[28].The competitive selectivity for C_2H_2/C_2H_4 and C_2H_6/C_2H_4 along with the high uptake of C_2H_2 and C_2H_6 at low pressure demonstrate exceedingly high performance in simultaneous removal of acetylene and ethane for ethylene purification.

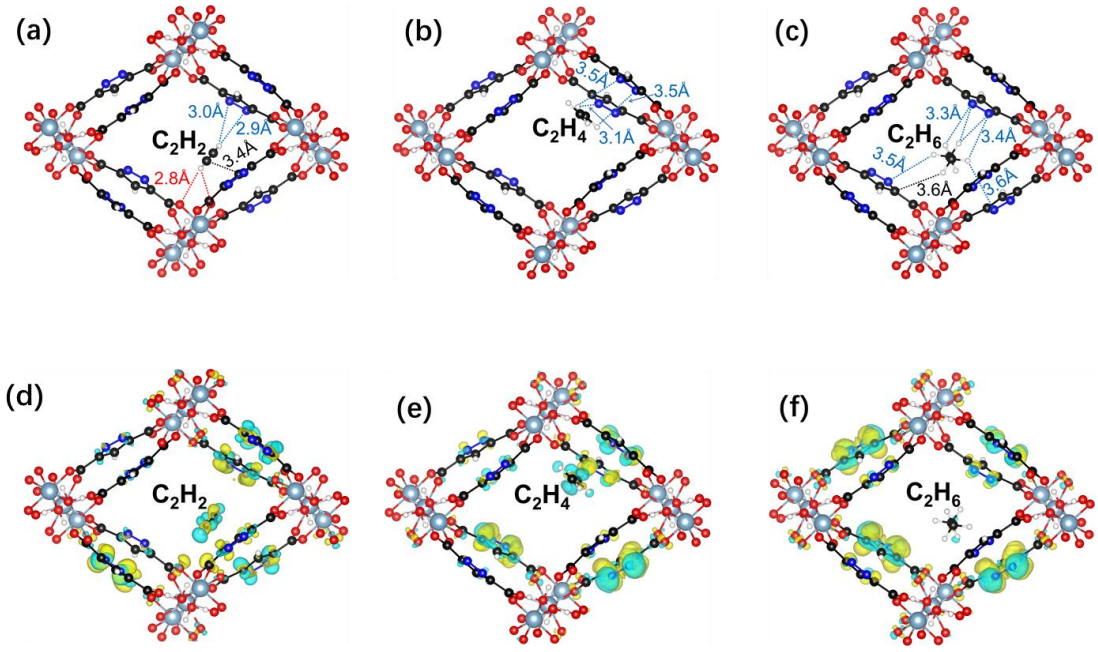

Fig. 4. The primary binding sites in MOF-303 structure for (a) C_2H_2, (b) C_2H_4, and (c) C_2H_6. Induced charge densities for (d) C_2H_2, (e) C_2H_4, and (f) C_2H_6, with iso-level of 0.001 electrons/Å3. The blue highlights represent the decrease in charge and yellow highlights show the increase in charge after binding of the molecules.

3.3 Theoretical calculations

To understand the mechanism of C_2 hydrocarbon adsorption on MOF-303, MIL-160, and CAU-23, density functional theory (DFT) calculations were performed. Fig. 4(a)-(c) show that the primary binding sites of C_2H_2, C_2H_4 and C_2H_6 are near the MOF linkers. The strongest interaction occurs with C_2H_2 and a binding energy of 97.6 kJ/mol was obtained. The binding energy of C_2H_6 was calculated to be 80.0 kJ/mol, larger than that of C_2H_4 (74.6 kJ/mol). The order of the binding energies ($C_2H_2 > C_2H_6 > C_2H_4$) coincides well with the experimental results, such as the zero coverage isosteric heats and the uptakes. As shown in Fig. 4(a), C_2H_2 interacts strongly with multiple linkers through N and O atoms. The induced charge densities plotted in Fig. 4(d) shows the interaction with the linker rings is primarily via π-bonds, where N atoms, located at a short distance from the acetylene, act as stronger adsorption sites compared to the C

atoms. The results also point towards a H-bond type interaction with the O atoms from the COO^- group (present at the metal cluster), resulting in a high binding energy for C_2H_2. In the case of C_2H_4, the molecule also interacts with linker rings but at longer distances (Fig. 4(b)), with the interaction concentrated at the C-H bonds (as shown by the induced charge densities, Fig. 4(e)), indicative of a much weaker binding strength. The C_2H_6 molecule at its primary binding site is shifted more towards the center of the pore due to its larger kinetic diameter (Fig. 4(c)). However, induced charge densities in Fig. 4(f) show that C_2H_6 interacts mainly with the N atoms of the linkers via C-H bonds, and the number of linkers involved in the interaction is higher than that of C_2H_4, resulting in a stronger interaction and higher binding energy. The binding energy calculations for MIL-160 showcase the binding strength order of C_2H_2 (52.3 kJ/mol) > C_2H_6 (50.9 kJ/mol) > C_2H_4 (46.2 kJ/mol), when binding at the primary binding site (Fig. S16). The induced charge densities, representing the redistribution of charge on binding, are also shown in Fig. S16. All three guest molecules prefer binding near the linkers, interacting primarily with the O atoms that are part of the linkers via their C-H bonds. The binding energy calculations for CAU-23 showcase the same trend as the case of MIL-160, with the binding energy of C_2H_2 (44.4 kJ/mol) > C_2H_6 (40.2 kJ/mol) > C_2H_4 (34.1 kJ/mol), at their primary binding sites located near the MOF linker (Fig. S17). The induced charge densities, representing the redistribution of charge on binding, are also shown in Fig. S17. Similar to the case for MIL-160, all three guest molecules have their primary binding site at the linkers, interacting primarily with the S atoms that are part of the linkers via their C—H bonds. The C_2H_6 molecule also has additional strong interaction with the O—H group at the metal cluster contributing to its larger binding energy.

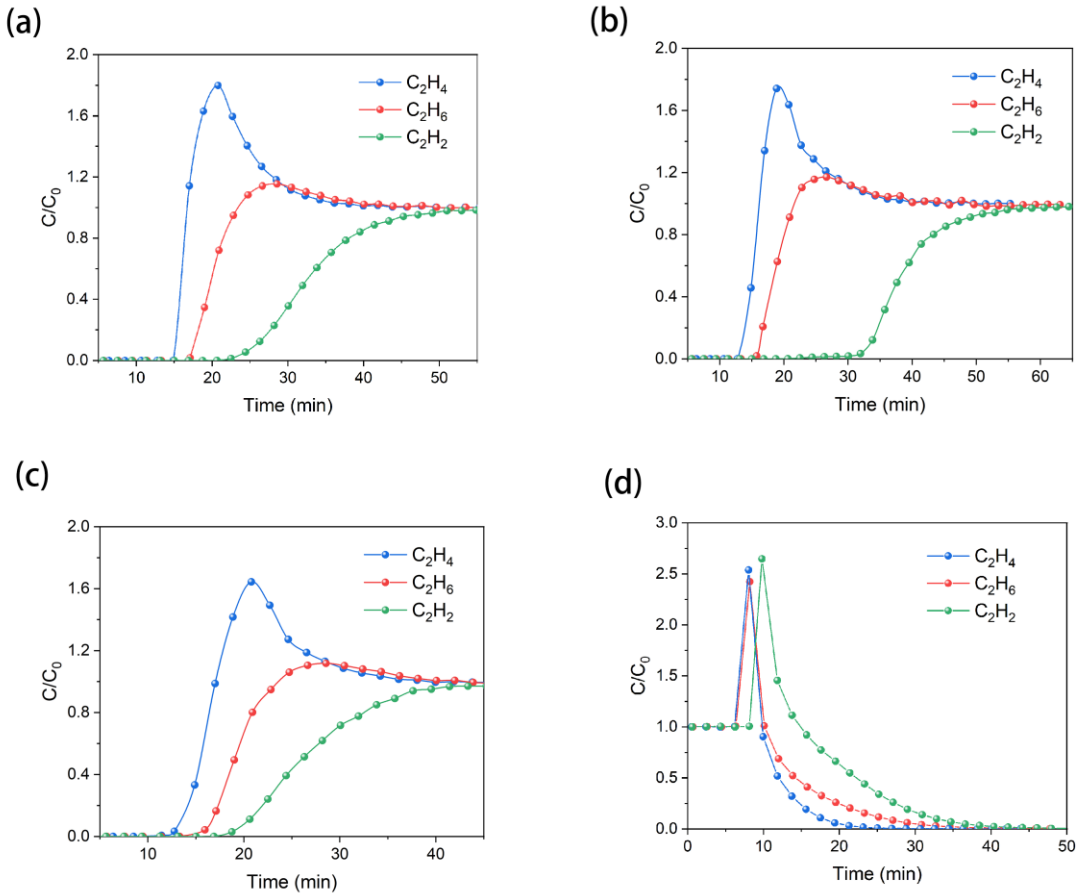

Fig. 5. Dynamic breakthrough curves for ternary gas mixture ($C_2H_6/C_2H_4/C_2H_2$, 1:1:1, v/v/v) on (a) MOF-303, (b) MIL-160, and (c) CAU-23 at 298 K and 100 kPa. (c) Desorption curves for MOF-303 packed column at 323 K under 5 mL/min He flow.

3.4 Breakthrough experiments and regeneration tests

To evaluate the separation potential of MOF-303, MIL-160, and CAU-23 under conditions similar to the industrial settings, dynamic breakthrough experiments were carried out on ternary ($C_2H_6/C_2H_4/C_2H_2$, 1:1:1, v/v/v) gas mixtures. As shown in Fig. 5(a), C_2H_4 eluted out first at 14.8 min, followed by C_2H_6 and C_2H_2 with a breakthrough time of 17 and 20.6 min, respectively, coinciding well with the isosteric heats and the theoretical calculation results. The relatively short interval between the breakthrough times for C_2H_4 and C_2H_6 are attributed to their similar isosteric heats and binding energies, and for C_2H_2, the higher isosteric heat and binding energy are responsible for the longer breakthrough time. In Fig. 5(b) and 5(c), similar curves with different

breakthrough times were observed. The breakthrough time of MIL-160 for C_2H_2 is more than 30 min, much longer than that of MOF-303 and CAU-23, consistent with the high C_2H_2 uptake and C_2H_2/C_2H_4 selectivity. As expected, the breakthrough times of CAU-23 for C_2H_2, C_2H_6, and C_2H_4 are the shortest among the three MOFs. In Fig. 5(a), before the breakthrough of C_2H_6, C_2H_4 of polymer-grade purity (> 99.9%) can be harvested, with the productivity of 0.164 mmol/g, confirming the ability of MOF-303 to produce polymer-grade C_2H_4 from 1:1:1 $C_2H_2/C_2H_4/C_2H_6$ in a single separation step. For MIL-160 and CAU-23, the productivity values are 0.21 and 0.181 mmol/g, respectively. For C_2H_4 productivity, MIL-160 is only comparable with MOF-303 and CAU-23 although its C_2H_2 uptake capacity and C_2H_2/CH_4 selectivity are impressive, which may be due to the similar C_2H_6/C_2H_4 selectivity among the three MOFs. In addition, owing to the strong affinity of C_2H_2, competitive adsorption between C_2H_2 and C_2H_6 molecule in MIL-160 may sharply shorten the C_2H_6 breakthrough time, leading to a reduced productivity of high-purity C_2H_4. The productivity of the three Al-MOFs greatly exceeds that of NPU-1(0.075 mmol/g) and NPU-2(~0.01 mmol/g)[24] but less than that of UPC-612 (0.47 mmol/g) and UPC-613 (0.34 mmol/g)[25] under the same experimental conditions. Although the C_2H_4 productivity of UPC-612 is more than twice of the amount of the three Al-MOFs, considering that the synthesis of TCBCBCPC, the ligand of UPC-612, is very complex and even the starting materials of TCBCBCPC are much more expensive than the ligands in MOF-303, MIL-160, and CAU-23, the latter group is much more suitable for industrial applications.

To evaluate the regeneration performance of MOM-303, MIL-160, and CAU-23, desorption curves were carried out at a low-cost condition, 323 K and 5 mL/min He flow, after a single separation step. As shown in Fig. 5(d), during the desorption process of MOF-303, C_2H_4, C_2H_6, and C_2H_2 can be fully removed in 28, 40, and 50 min, respectively, demonstrating that MOF-303 column can be fully activated by heating at 323 K for 50 min. For MIL-160 and CAU-23, the fully active times are 65 and 40 min, as shown in Figs. S25-S26, which suggests CAU-23 is more promising when used for simultaneous removal of acetylene and ethane for ethylene purification compared to

MOF-303 because of the higher polymer-grade C_2H_4 productivity and the lower regeneration energy cost. Finally, binary gas mixture breakthrough experiments were also conducted for another 4 adsorption-desorption cycles consecutively to further test the recycling performance of MOF-303, MIL-160, and CAU-23. As illustrated in Figs. S27-S29, the breakthrough time for C_2H_4 remains nearly constant, consistent with the results of 10 continuous C_2H_6 adsorption-desorption cycles on all three MOFs measured at 298 K (Fig. S30). These results provide solid evidence of the excellent stability of the three MOFs.

To evaluate how water molecules may affect the purification of ethylene, we further carried out breakthrough experiments for a ternary gas mixture ($C_2H_6/C_2H_4/C_2H_2$, 1:1:1, v/v/v) on MOF-303 under 45% RH, as shown in Fig. S31. Except for the humidity, other experiment conditions are the same as the conditions shown in part 2.5 in the manuscript. Compared with the separation at dry condition, the three gases follow the same breakout order, but with decreased breakthrough times, owning to the competitive water adsorption (Table S11). We found the duration between the C_2H_4 and C_2H_6 breakthrough that determine the yield of high purity ethylene under 45% RH is 182 s, nearly the same with that in dry condition, 180 s, suggesting that 45% RH condition have no effect on the yield of high purity ethylene, although the uptake of C_2H_4, C_2H_6, and C_2H_2 are reduced by the competitive adsorption of water. Similarly, the yield of high purity ethylene for MIL-160 and CAU-23 may not be affected by water vapour, but the adsorbed amounts would be decrease remarkably due to the hydrophilic frameworks. These results further confirm that MOF-303, MIL-160, and CAU-23 are promising adsorbent for simultaneous removal of C_2H_6 and C_2H_2 from C_2H_4 streams.

Conclusion

Three highly stable Al-based MOFs, MOF-303, MIL-160, and CAU-23 were investigated for C2 hydrocarbon separations. All three ethane-selective MOFs show high C_2H_6 uptake and good C_2H_6/C_2H_4 selectivity. Notably, the C_2H_6 uptake in MOF-303, MIL-160 and CAU-23 are up to 4.96, 4.65, and 4.3mmol/g at 298 K and 1 bar,

outperforming most ethane-selective MOFs reported to date. Taking into consideration of their ultrahigh C_2H_2 adsorption capacity at low pressure (e.g., 0.1 bar), 2.42 mmol/g for MOF-303, 4.01 mmol/g for MIL-160, and 1.67 mmol/g for CAU-23, and excellent C_2H_2/C_2H_4 selectivity, 2.45, 10.46, and 2.06, respectively, we further assessed their ability to simultaneously remove C_2H_6 and C_2H_2 from C_2H_4. Our results from breakthrough experiments on these Al-MOFs show that polymer-grade high-purity C_2H_4 can be achieved in one step from a ternary mixture of $C_2H_2/C_2H_4/C_2H_6$, with a productivity of 0.164, 0.21, and 0.181mmol/g, respectively for MOF-303, MIL-160, and CAU-23, higher than some of the best-performing MOFs, such as NPU-1 and NPU-2. The MOF-filled columns can be fully activated/regenerated at moderate temperature (50 °C or 323 K) in less than 65 min, and no sign of degradation was detected in four cycles. DFT calculations reveal that the strong affinity between C_2H_6 (or C_2H_2) and the heteroatom of the linker molecules gives rise to the high loading capacity and selectivity for C_2H_2 and C_2H_6. Overall, the three Al-based MOFs, MOF-303, MIL-160, and CAU-23 represent promising candidates for industrial adsorptive C_2H_4 purification with a good balance on stability, cost, and performance.

Acknowledgements

We would like to thank the U. S. Department of Energy, Office of Science, Office of Basic Energy Sciences (Grant No. DE-SC0019902) for the partial support of this work. S. Xian, J. Peng and H. Wang acknowledge the financial support from National Natural Science Foundation of China (No. 21908069, 21901166), Guangdong Natural Science Foundation (2019A1515010692), and Shenzhen Science and Technology Program (No. JCYJ20190809145615620, RCYX20200714114539243).

References

1. I. Amghizar, L. A. Vandewalle, K. M. Van Geem and G. B. Marin, *Engineering*, 2017, **3**, 171-178.
2. Y. He, R. Krishna and B. Chen, *Energy & Environmental Science*, 2012, **5**, 9107-9120.
3. H. Molero, B. F. Bartlett and W. T. Tysoe, *Journal of Catalysis*, 1999, **181**, 49-56.
4. H.-G. Hao, Y.-F. Zhao, D.-M. Chen, J.-M. Yu, K. Tan, S. Ma, Y. Chabal, Z.-M. Zhang,

J.-M. Dou, Z.-H. Xiao, G. Day, H.-C. Zhou and T.-B. Lu, *Angewandte Chemie International Edition*, 2018, **57**, 16067-16071.

5. Z. Xu, X. Xiong, J. Xiong, R. Krishna, L. Li, Y. Fan, F. Luo and B. Chen, *Nature Communications*, 2020, **11**, 3163.
6. B. Wang, L.-H. Xie, X. Wang, X.-M. Liu, J. Li and J.-R. Li, *Green Energy & Environment*, 2018, **3**, 191-228.
7. O. T. Qazvini, R. Babarao, Z.-L. Shi, Y.-B. Zhang and S. G. Telfer, *Journal of the American Chemical Society*, 2019, **141**, 5014-5020.
8. P.-Q. Liao, W.-X. Zhang, J.-P. Zhang and X.-M. Chen, *Nature Communications*, 2015, **6**, 8697.
9. W.-G. Cui, T.-L. Hu and X.-H. Bu, *Advanced Materials*, 2020, **32**, 1806445.
10. J.-R. Li, J. Yu, W. Lu, L.-B. Sun, J. Sculley, P. B. Balbuena and H.-C. Zhou, *Nature Communications*, 2013, **4**, 1538.
11. R.-B. Lin, L. Li, H.-L. Zhou, H. Wu, C. He, S. Li, R. Krishna, J. Li, W. Zhou and B. Chen, *Nature Materials*, 2018, **17**, 1128-1133.
12. S. Yang, A. J. Ramirez-Cuesta, R. Newby, V. Garcia-Sakai, P. Manuel, S. K. Callear, S. I. Campbell, C. C. Tang and M. Schröder, *Nature Chemistry*, 2015, **7**, 121-129.
13. P. Verma, X. Xu and D. G. Truhlar, *The Journal of Physical Chemistry C*, 2013, **117**, 12648-12660.
14. X. Wang, Y. Wu, J. Peng, Y. Wu, J. Xiao, Q. Xia and Z. Li, *Chemical Engineering Journal*, 2019, **358**, 1114-1125.
15. Y. Chang, H. Huang, H. Zhu, Y. Zhao, L. Wang, Y. Sun and C. Zhong, *Chemical Engineering Journal*, 2022, **427**, 131726.
16. S. J. Geier, J. A. Mason, E. D. Bloch, W. L. Queen, M. R. Hudson, C. M. Brown and J. R. Long, *Chemical Science*, 2013, **4**, 2054-2061.
17. S. Horike, Y. Inubushi, T. Hori, T. Fukushima and S. Kitagawa, *Chemical Science*, 2012, **3**, 116-120.
18. D.-L. Chen, N. Wang, C. Xu, G. Tu, W. Zhu and R. Krishna, *Microporous and Mesoporous Materials*, 2015, **208**, 55-65.
19. D. Lv, R. Shi, Y. Chen, Y. Wu, H. Wu, H. Xi, Q. Xia and Z. Li, *ACS Applied Materials & Interfaces*, 2018, **10**, 8366-8373.
20. Y. Chen, Z. Qiao, H. Wu, D. Lv, R. Shi, Q. Xia, J. Zhou and Z. Li, *Chemical Engineering Science*, 2018, **175**, 110-117.
21. S. Geng, E. Lin, X. Li, W. Liu, T. Wang, Z. Wang, D. Sensharma, S. Darwish, Y. H. Andaloussi, T. Pham, P. Cheng, M. J. Zaworotko, Y. Chen and Z. Zhang, *Journal of the American Chemical Society*, 2021, **143**, 8654-8660.
22. L. Yang, Y. Wang, Y. Chen, J. Yang, X. Wang, L. Li and J. Li, *Chemical Engineering Journal*, 2020, **387**, 124137.
23. T.-L. Hu, H. Wang, B. Li, R. Krishna, H. Wu, W. Zhou, Y. Zhao, Y. Han, X. Wang, W. Zhu, Z. Yao, S. Xiang and B. Chen, *Nature Communications*, 2015, **6**, 7328.
24. B. Zhu, J.-W. Cao, S. Mukherjee, T. Pham, T. Zhang, T. Wang, X. Jiang, K. A. Forrest, M. J. Zaworotko and K.-J. Chen, *Journal of the American Chemical Society*, 2021, **143**, 1485-1492.
25. Y. Wang, C. Hao, W. Fan, M. Fu, X. Wang, Z. Wang, L. Zhu, Y. Li, X. Lu, F. Dai, Z.

Kang, R. Wang, W. Guo, S. Hu and D. Sun, *Angewandte Chemie International Edition*, 2021, **60**, 11350-11358.
26. S. Xiang, W. Zhou, J. M. Gallegos, Y. Liu and B. Chen, *Journal of the American Chemical Society*, 2009, **131**, 12415-12419.
27. J. Pang, F. Jiang, M. Wu, C. Liu, K. Su, W. Lu, D. Yuan and M. Hong, *Nature Communications*, 2015, **6**, 7575.
28. H.-M. Wen, H. Wang, B. Li, Y. Cui, H. Wang, G. Qian and B. Chen, *Inorganic Chemistry*, 2016, **55**, 7214-7218.
29. T. Ke, Q. Wang, J. Shen, J. Zhou, Z. Bao, Q. Yang and Q. Ren, *Angewandte Chemie International Edition*, 2020, **59**, 12725-12730.
30. R.-B. Lin, L. Li, H. Wu, H. Arman, B. Li, R.-G. Lin, W. Zhou and B. Chen, *Journal of the American Chemical Society*, 2017, **139**, 8022-8028.
31. X.-J. Kong and J.-R. Li, *Engineering*, 2021, **7**, 1115-1139.
32. D. Lv, J. Chen, Y. Chen, Z. Liu, Y. Xu, C. Duan, H. Wu, Y. Wu, J. Xiao, H. Xi, Z. Li and Q. Xia, *AIChE Journal*, 2019, **65**, e16616.
33. A. N. Hong, H. Yang, T. Li, Y. Wang, Y. Wang, X. Jia, A. Zhou, E. Kusumoputro, J. Li, X. Bu and P. Feng, *ACS Applied Materials & Interfaces*, 2021, **13**, 52160-52166.
34. H. Yang, Y. Wang, R. Krishna, X. Jia, Y. Wang, A. N. Hong, C. Dang, H. E. Castillo, X. Bu and P. Feng, *Journal of the American Chemical Society*, 2020, **142**, 2222-2227.
35. F. Fathieh, M. J. Kalmutzki, E. A. Kapustin, P. J. Waller, J. Yang and O. M. Yaghi, *Science Advances*, 2018, **4**, eaat3198.
36. G. Kresse and J. Furthmüller, *Physical Review B*, 1996, **54**, 11169-11186.
37. G. Kresse and D. Joubert, *Physical Review B*, 1999, **59**, 1758-1775.
38. K. Berland, V. R. Cooper, K. Lee, E. Schröder, T. Thonhauser, P. Hyldgaard and B. I. Lundqvist, *Reports on Progress in Physics*, 2015, **78**, 066501.
39. D. C. Langreth, B. I. Lundqvist, S. D. Chakarova-Käck, V. R. Cooper, M. Dion, P. Hyldgaard, A. Kelkkanen, J. Kleis, L. Kong, S. Li, P. G. Moses, E. Murray, A. Puzder, H. Rydberg, E. Schröder and T. Thonhauser, *Journal of Physics: Condensed Matter*, 2009, **21**, 084203.
40. T. Thonhauser, V. R. Cooper, S. Li, A. Puzder, P. Hyldgaard and D. C. Langreth, *Physical Review B*, 2007, **76**, 125112.
41. T. Thonhauser, S. Zuluaga, C. A. Arter, K. Berland, E. Schröder and P. Hyldgaard, *Physical Review Letters*, 2015, **115**, 136402.
42. L. Li, R.-B. Lin, R. Krishna, H. Li, S. Xiang, H. Wu, J. Li, W. Zhou and B. Chen, *Science*, 2018, **362**, 443.
43. R.-B. Lin, H. Wu, L. Li, X.-L. Tang, Z. Li, J. Gao, H. Cui, W. Zhou and B. Chen, *Journal of the American Chemical Society*, 2018, **140**, 12940-12946.
44. W. Liang, F. Xu, X. Zhou, J. Xiao, Q. Xia, Y. Li and Z. Li, *Chemical Engineering Science*, 2016, **148**, 275-281.
45. S. Xiang, W. Zhou, Z. Zhang, M. A. Green, Y. Liu and B. Chen, *Angewandte Chemie International Edition*, 2010, **49**, 4615-4618.